

Measurement of the acoustic scatterers distribution within the imaged sample in an optoacoustic tomographic setup

X Luís Deán-Ben, Daniel Razansky and Vasilis Ntziachristos*

Institute for Biological and Medical Imaging, Technical University of Munich and Helmholtz Center Munich, Ingolstädter Landstraße 1, 85764 Neuherberg, Germany.

ABSTRACT

We present in this work a method to estimate the distribution of acoustic scatterers within the imaged sample in an optoacoustic tomographic setup and, subsequently, to reduce the artefacts in the tomographic reconstructions due to reflection or scattering events. The procedure to determine the position of the scatterers consists of measuring the scattered waves generated at a point light absorber located in between the transducer and the imaged sample. Such absorber is positioned in a way that the acoustic waves generated at this absorber and scattered within the sample arrive at the position of the transducer after the waves generated within the sample that propagate directly until the measuring point. Then, the signals captured by the acoustic transducer can be used to reconstruct the distribution of acoustic scatterers and to perform the optoacoustic reconstruction itself. Also, the information retrieved on the distribution of acoustic scatterers can be used to improve the optoacoustic tomographic reconstructions. For this, we use a modification of the filtered back-projection algorithm based on weighting the signals with the probability that they are not affected by scattered or reflected waves, so that the artefacts in the images due to these acoustic phenomena are reduced. The experimental results obtained with a tissue-mimicking phantom in which a straw filled with air was included in order to cause scattering of the acoustic waves indicate a good performance of the method proposed.

Keywords: Optoacoustic tomography, weighted back-projection algorithm, acoustic scattering

1. INTRODUCTION

Optoacoustic tomography (OAT), also referred to as photoacoustic tomography, is a noninvasive imaging modality capable of mapping the optical absorption in tissues with a higher resolution than pure optical techniques for depths of several millimetres to centimetres of tissue.¹ OAT presents important advantages derived from the synergetic combination of optics and ultrasound in a single modality. Thus, the absorption of light by tissue chromophores provides high contrast and the measured ultrasonic signals provide high resolution. Using imaging at different optical wavelengths, OAT has further shown the capability of functional and molecular imaging.^{2,3}

In OAT, the optical source is usually a short-pulsed laser with a pulse duration verifying thermal confinement conditions. In such case, the optoacoustic reconstruction consists of calculating the initial pressure, which is proportional to the optical absorbed energy, from the measured pressure at several positions outside the sample. For this, several algorithms have been suggested, in which for simplicity a uniform medium with no acoustic mismatch is assumed.⁴⁻⁷ However, in a general case the acoustic impedance varies for different tissues, so this simplification may affect the quality of the reconstructions. In general, the density and the speed of sound within biological tissues are space-dependent, and different effects take place along the propagation path of the ultrasonic waves depending on the degree of acoustic heterogeneity. Thus, for small variations in the speed of sound, the waves are usually assumed to propagate along straight acoustic rays, so that the main effect of the heterogeneities is the time-shifting of the optoacoustic signals.⁸ On the other hand, other acoustic phenomena such as scattering or reflections of the ultrasonic waves occur in the interfaces between regions with a higher acoustic mismatch, which cause artefacts in the images obtained with standard reconstruction algorithms.⁹

A procedure to minimize the effects of scattering and reflections of the acoustic waves in the tomographic reconstructions consists of performing the reconstruction preferably with the signals less affected by these phenomena. Thereby, the contribution of a signal measured at a given instant and at a given position is weighted

*E-mail: vntziachristos@gmail.com

with the probability that such signal is not affected by a reflected or scattered acoustic wave. The accuracy in the estimation of such probability depends on the available information on the inner structure of the sample, specifically on the distribution of optical absorbers and acoustic scatterers. In a first order approximation, we assumed that the location of optical absorbers and acoustic scatterers corresponds to a uniform probability distribution inside an area covering the sample.⁹ Whereas the reduction of artefacts in the images obtained with this approach was significant, it was not possible to remove the artefacts located close to the middle of the sample, as for those points the weighting of the signals is the same for all the positions of the transducer. In a different work,¹⁰ we showed that the results can be further improved if a more confined area covering all the acoustic scatterers is determined. Therefore, it may be convenient in some cases to make an *a priori* estimation of the distribution of acoustic scatterers in order to reduce the artefacts due to acoustic distortion events.

In this work, we introduce a method to estimate the distribution of acoustic scatterers inside a sample being measured with an optoacoustic tomographic setup. For this, we introduce a strong optical absorber between the sample and the transducer, so that the acoustic waves generated at this absorber and scattered within the sample are detected at the transducer after the waves generated within the sample and propagating directly until the measuring point. Thereby, it is possible to use the signals captured by the acoustic transducer both to reconstruct the distribution of acoustic scatterers and to perform the optoacoustic reconstruction itself. The organization of this work is as follows, in section 2 we review theoretically the filtered back-projection algorithm with and without weighting the contribution of each signal. The expressions for the probability that a signal is not affected by a reflected or scattered acoustic wave, which is the basis of the weighting, are also reviewed. In section 3 we introduce the method to measure the distribution of acoustic scatterers inside the sample. More precisely, we explain the changes in the tomographic optoacoustic setup and we suggest a reconstruction procedure from the measured signals. The experimental results are shown in section 4 and finally some concluding remarks are made in section 5.

2. THEORETICAL BACKGROUND

2.1 Filtered back-projection algorithm

The optoacoustic effect refers to the generation of acoustic waves by the thermoelastic expansion caused by the absorption of light energy within a sample. The theoretical basis of the optoacoustic generation of ultrasonic waves inside a medium is well-known and can be found in the literature.¹¹ Typically, a short-pulsed laser is used as the illumination source, so that thermal confinement conditions are verified and the temporal dependence of the light intensity at any point can effectively be expressed as a Dirac delta $\delta(t)$. Under these conditions, the pressure field $p(\mathbf{r}, t)$ caused by the propagation of the generated ultrasonic wave in a homogeneous acoustic medium satisfies

$$\frac{\partial^2 p(\mathbf{r}, t)}{\partial t^2} - c^2 \nabla^2 p(\mathbf{r}, t) = \Gamma H(\mathbf{r}) \frac{\partial \delta(t)}{\partial t}, \quad (1)$$

where $H(\mathbf{r})$ is the optical absorption field, i.e., the amount of energy absorbed in the tissue per unit volume, Γ is the dimensionless Grueneisen parameter and c is the speed of sound in the medium. The pressure field is then given by Poisson's solution of Eq. 1 as

$$p(\mathbf{r}, t) = \frac{\Gamma}{4\pi c} \frac{\partial}{\partial t} \int_{S'} \frac{H(\mathbf{r}')}{|\mathbf{r} - \mathbf{r}'|} dS', \quad (2)$$

where S' is a spherical surface verifying $|\mathbf{r} - \mathbf{r}'| = ct$. Eq. 2 indicates that the pressure $p(\mathbf{r}, t)$ caused by an optoacoustic wave propagating in a homogeneous acoustic medium is solely determined by the optical absorption at locations \mathbf{r}' so that the generated waves require time t to reach \mathbf{r} .

The optoacoustic reconstruction consists in retrieving the distribution of $H(\mathbf{r}')$ from the value of the pressure recorded at a set of points outside the imaged sample. For this, several back-projection algorithms have been developed,^{7,12} which are commonly employed due to their ease of implementation. In a universal back-projection algorithm for homogeneous acoustic media,⁷ the optical absorption field is given by

$$H(\mathbf{r}') = \frac{1}{\Gamma} \int_{\Omega} \frac{d\Omega}{\Omega} \left[2p(\mathbf{r}, t) - 2t \frac{\partial p(\mathbf{r}, t)}{\partial t} \right] \Big|_{t=|\mathbf{r}-\mathbf{r}'|/c}. \quad (3)$$

In principle, Eq. 3 is deduced for a surface S enclosing \mathbf{r}' , i.e., the solid angle $\Omega = 4\pi$. $d\Omega$ is the solid angle for an element dS and acts as a weighting factor in the reconstruction. The reconstruction procedure consists in projecting the value of the quantity $2p(\mathbf{r}, t) - 2t\partial p(\mathbf{r}, t)/\partial t$ for a given instant t and for a given point \mathbf{r} back onto the spherical surface where a wave should be generated to reach the point \mathbf{r} at instant t according to Eq. 2.

In some experimental cases, a two-dimensional geometry can be considered, for which the optoacoustic sources lie in a plane. For this, a cylindrically focused ultrasonic transducer can for example be used to measure the outgoing pressure waves around a circumference of the object.^{12, 13} In this case, a 2D cross section of the sample can be imaged with an approximate solution for the circular-scan geometry by considering the back-projection algorithm in a 2D geometry.¹² Furthermore, if the scanning radius is much larger than the size of the object, the angle covered by each transducer is approximately constant. Under these conditions, a 2D discretization of Eq. 3, in which for simplicity all the constants are dropped, is given by

$$H(\mathbf{r}'_j) = \sum_i \left[p(\mathbf{r}_i, t_{ij}) - t_{ij} \frac{\partial p(\mathbf{r}_i, t_{ij})}{\partial t} \right], \quad (4)$$

where \mathbf{r}_i is the position of i -th transducer, \mathbf{r}'_j is the position of the j -th point of the reconstruction region of interest and $t_{ij} = |\mathbf{r}_i - \mathbf{r}'_j|/c$.

2.2 Statistical weighting

In this section we review the modification of the filtered back-projection algorithm based on weighting the signals with the probability that the signals are not affected by acoustic reflection or scattering events. We introduce the expressions for such probability in two possible scenarios, namely when considering an area covering all the optical absorbers and acoustic scatterers and when a more confined area covering all the acoustic scatterers can be determined. A more detailed description can be found in Refs. 9 and 10.

The proposed variant of the filtered back-projection reconstruction algorithm consists of weighting the optoacoustic signals with the probability $P_d^i(t_{ij})$ that a signal measured with the i -th transducer at instant t_{ij} corresponds to a direct wave propagation and is not distorted by reflected or scattered waves. This is done in a way that Eq. 4 is modified as follows:

$$H(\mathbf{r}'_j) = \sum_i P_d^i(t_{ij}) \left[p(\mathbf{r}_i, t_{ij}) - t_{ij} \frac{\partial p(\mathbf{r}_i, t_{ij})}{\partial t} \right]. \quad (5)$$

The value of $P_d^i(t_{ij})$ is given by

$$P_d^i(t_{ij}) = 1 - P_{r,dist}^i(t_{ij}), \quad (6)$$

being $P_{r,dist}^i(t_{ij})$ the probability that the signal measured by the i -th transducer at instant t_{ij} is distorted by a reflected or scattered wave. In practice, the measured wave is distorted when the amplitude of the reflected or scattered wave is above the noise level, so that $P_{r,dist}^i(t_{ij})$ is proportional to $P_r^i(t_{ij})$, being $P_r^i(t_{ij})$ the probability that a reflected or scattered wave with unit amplitude (in arbitrary units) is detected by the i -th transducer at time t_{ij} . According to Bayes' theorem, $P_r^i(t_{ij})$ can be expressed as

$$P_r^i(t_{ij}) = \int_A P_r^i(t_{ij}|\mathbf{r}') f_E(\mathbf{r}') d\mathbf{r}', \quad (7)$$

where $P_r^i(t_{ij}|\mathbf{r}')$ is the conditional probability that a reflected or scattered wave with unit amplitude is detected at t_{ij} given that all the energy absorbed by the sample is entirely absorbed at \mathbf{r}' . If no information on the distribution of optical absorbers is available, we can assume that $f_E(\mathbf{r}')$ corresponds to a uniform probability distribution inside an area A covering the sample (Fig. 1). In such case, Eq. 7 can be expressed as

$$P_r^i(t_{ij}) = \frac{1}{A} \int_{A_{ij}} P_r^i(t_{ij}|\mathbf{r}') d\mathbf{r}', \quad (8)$$

where A_{ij} is an area in which the signal must be generated in order to reach the transducer at t_{ij} either by propagating directly to the transducer or undergoing reflection or scattering events (dashed area in Fig. 1a).

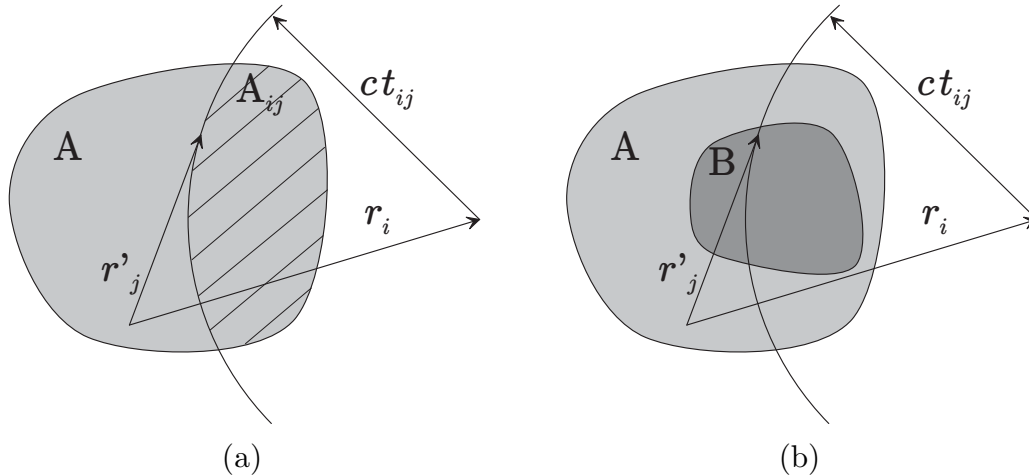


Figure 1. Underlying principle of the statistical weighting. In (a) we assume that the optical absorbers and the acoustic scatterers are randomly located inside the area A. In (b) we assume that the optical absorbers are randomly located inside the area A and that the acoustic scatterers are randomly located inside the area B.

On the other hand, the available knowledge on the distribution of acoustic scatterers conditions the accuracy in the estimation of $P_r^i(t_{ij})$. Fig. 1 illustrates two different scenarios. In Fig. 1a we assume that both the optical absorbers and the acoustic scatterers are randomly located inside the area A. In such case, Eq. 8 can be approximated as⁹

$$P_r^i(t_{ij}) = k_1 \frac{A_{ij}}{A}. \quad (9)$$

Then, considering that probability values should not be higher than 1, $P_{r,dist}^i(t_{ij})$ is given by

$$P_{r,dist}^i(t_{ij}) = \min \left(1, \omega \frac{A_{ij}}{A} \right). \quad (10)$$

Fig. 1b shows a different case in which an area B inside A covering all the acoustic scatterers can be determined. In such case, Eq. 8 can be expressed as

$$P_r^i(t_{ij}) = \frac{k_2}{A} \int_A \left[\int_B \delta(t_r^i(\mathbf{r}', \mathbf{r}'') - t_{ij}) d\mathbf{r}'' \right] d\mathbf{r}', \quad (11)$$

being $\delta()$ the one dimensional Dirac delta and $t_r^i(\mathbf{r}', \mathbf{r}'') = |\mathbf{r}' - \mathbf{r}''|/c + |\mathbf{r}'' - \mathbf{r}_i|/c$, i.e., the instant at which a wave generated at \mathbf{r}' and reflected or scattered at \mathbf{r}'' is detected by the i -th transducer.

Eq. 11 indicates that two points \mathbf{r}' and \mathbf{r}'' in A and B, respectively, contribute to $P_r^i(t_{ij})$ for $t_{ij} = t_r^i(\mathbf{r}', \mathbf{r}'')$. In Ref. 10, we suggested to estimate the shape of $P_r^i(t_{ij})$ by means of the Monte Carlo method, generating randomly n pairs of points $(\mathbf{r}', \mathbf{r}'')$ in A and B and calculating the corresponding values of $t_r^i(\mathbf{r}', \mathbf{r}'')$. If the value of n is large enough, the histogram of $t_r^i(\mathbf{r}', \mathbf{r}'')$ faithfully represents the shape of $P_r^i(t_{ij})$. We defined the function $P_{r,hist}^i(t_{ij})$ in the centres of the intervals of the histogram as the number of elements N in such intervals. For the rest of points, the value of $P_{r,hist}^i(t_{ij})$ is obtained by linear interpolation. Subsequently, taking into account that $P_{r,dist}^i(t_{ij})$ is proportional to $P_r^i(t_{ij})$ and probability values should not exceed unity, one could estimate $P_{r,dist}^i(t_{ij})$ as

$$P_{r,dist}^i(t_{ij}) = \min \left(1, \omega \frac{P_{r,hist}^i(t_{ij})}{\max_{i,j} [P_{r,hist}^i(t_{ij})]} \right). \quad (12)$$

Both Eq. 10 and Eq. 12 are expressed as a function of a weighting parameter ω . Such parameter depends on the initial features of the sample and can be determined heuristically. For example, in a sample in which

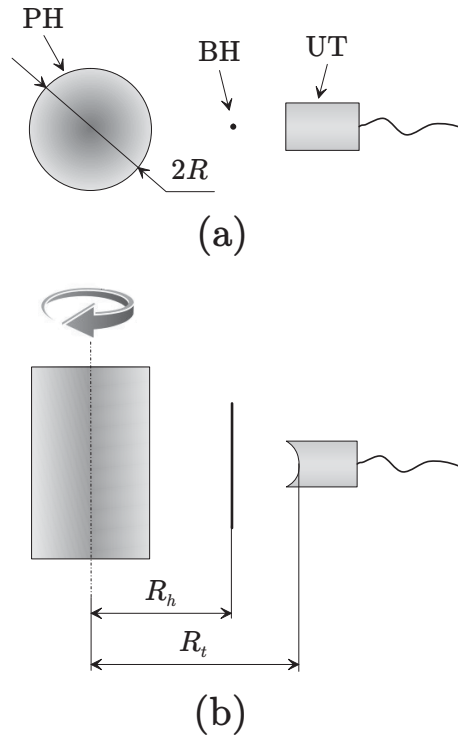


Figure 2. Layout of the experimental setup used to measure the distribution of acoustic scatterers. Basically an optical point absorber (a black hair (BH) in our case) is introduced in between the ultrasonic transducer (UT) and the imaging sample (a tissue-mimicking phantom (PH) in our case). (a) Top view. (b) Lateral view.

reflections or scattering are very likely to occur, ω has a high value whereas in a sample with very few reflectors or scatterers ω approaches 0.

3. MATERIALS AND METHODS

3.1 Experimental setup

The experimental setup used to measure the distribution of acoustic scatterers consists of introducing a strong optical point absorber in between the transducer and the sample in a tomographic optoacoustic setup.

The tomographic optoacoustic setup is described in detail in Ref. 13. Basically, an optical parametric oscillator (OPO)-based laser (MOPO series, Spectra Physics), pumped by a nanosecond pulsed Nd:YAG laser (Lab-190-30, Spectra-Physics) with 15 Hz pulse repetition, was used as illumination source at a wavelength of 605 nm. The output beam was shaped with optical elements so that ring-type uniform illumination conditions were achieved at the surface of the sample. The generated ultrasonic waves were detected with a cylindrically-focused ultrasonic immersion PZT transducer (model V382, Panametrics-NDT, Waltam, MA) with a center frequency of 3.5 MHz and a focal length of 38.1 mm. The captured time-resolved signals were then amplified and digitized by an embedded oscilloscope card at a sampling rate of 100 MSPS (NI PCI-5122, National Instruments) and 14 bit resolution. A band-pass filter with cut-off frequencies of 0.1 and 5 MHz was then applied to the signals. The sample was rotated with a high speed rotation stage (Thorlabs PRM1/M-Z7) with angular steps of 2° along a whole circumference, so that 180 tomographic projections were acquired.

As an optical point absorber, we used a black hair as shown in Fig. 2. The hair has an approximate diameter of $80 \mu\text{m}$, so that it can be considered a point acoustic source for the frequency range of the transducer employed. It was positioned in a way that the waves generated at the hair and scattered within the sample arrive at the position of the transducer after the waves generated inside the sample and propagating directly until the

transducer. Specifically, the transducer was located at a distance from the rotation centre approximately equal to the focal length, i.e., $R_t \approx 38.1$ mm and the imaging samples typically have a radius lower than $R = 10$ mm. Then, the hair was introduced at a distance $R_h \approx 30$ mm from the rotation centre. Under these circumstances, the waves generated at the hair and scattered within the sample arrive at the transducer at time instants higher than $t_s = (R_h - R)/c + (R_t - R)/c$, which corresponds to a wave being scattered at the point of the sample closest to the position of the transducer. On the other hand, the ultrasonic waves generated within the sample and propagating directly to the transducer arrive at the transducer at time instants lower than $t_d = (R + R_t)/c$, which corresponds to a wave generated at the point of the sample further from the position of the transducer. Provided $t_s \geq t_d$, or equivalently $R_h \geq 3R$, the part of the signal corresponding to the waves generated at the point absorber and scattered within the sample can be isolated from the rest of the signal. Although this part of the signal may be affected by the waves generated within the sample that undergo scattering or reflection events, their effect can be neglected as the wave generated at the point absorber has typically a much higher amplitude than the waves generated within the sample.

3.2 Reconstruction

A reconstruction procedure must be developed in order to obtain information about the distribution of acoustic scatterers inside the sample from the tomographic measurements of the scattered waves generated at the point absorber. In this work, we suggest an heuristic approach based on a modification of the filtered back-projection algorithm described in section 2.1.

As mentioned above, the procedure to perform the optoacoustic reconstruction with the filtered back-projection algorithm consists of projecting the value of the quantity $2p(\mathbf{r}, t) - 2t\partial p(\mathbf{r}, t)/\partial t$ for a given point and for a given instant back onto the points in which the wave must have been generated to be detected at the position of the transducer at that instant, i.e., such quantity is back-projected along a circumference centered at the position of the transducer. In our case, as the position of the point absorber \mathbf{r}_h is known, the same concept can be applied to do the reconstruction of the distribution of scatterers. In this way, we suggest to back-project the same quantity back onto the points in which the waves must have been scattered to be detected at point \mathbf{r} at instant t . Thereby, the distribution of acoustic scatterers $S(\mathbf{r}'_j)$ can be estimated as

$$S(\mathbf{r}'_j) = - \sum_i \left[p(\mathbf{r}_i, t_{hji}) - t_{hji} \frac{\partial p(\mathbf{r}_i, t_{hji})}{\partial t} \right], \quad (13)$$

where \mathbf{r}_i is the position of i -th transducer, \mathbf{r}'_j is the position of the j -th point of the reconstruction region of interest and $t_{hji} = |\mathbf{r}_h - \mathbf{r}'_j|/c + |\mathbf{r}'_j - \mathbf{r}_i|/c$, i.e., the back-projection is done along an ellipse whose foci are located at the position of the transducer and at the position of the optical absorber. The minus sign in Eq. 13 is introduced to correct for the pressure inversion that takes place for the phantom described below when the waves are reflected in the hollow cavity.

3.3 Phantom

A tissue-mimicking phantom was used in the experiment. It was made with an agar solution (1.3% agar powder by weight). The background optical absorption and the background optical scattering were simulated by adding 0.002% by volume of black India ink and 1.2% by volume of Intralipid to the agar solution, in a way that the optical absorption coefficient and the reduced scattering coefficient of the sample were, respectively, $\mu_a = 0.2 \text{ cm}^{-1}$ and $\mu'_s = 10 \text{ cm}^{-1}$. Areas with higher optical absorption and a hollow cylindrical cavity were included in the phantom. The concentration of ink (by volume) in the high absorbing areas was 0.02%, which is equivalent to an optical absorption coefficient of $\mu_a = 2 \text{ cm}^{-1}$. The hollow cavity was included to cause the scattering of the acoustic waves. A straw filled with air was introduced into such cavity in order to avoid water permeating into it when introducing the phantom inside the water tank.

4. EXPERIMENTAL RESULTS

The experimental results obtained with the phantom are displayed in Fig. 3. Fig. 3a shows the tomographic reconstruction of the phantom obtained with the classical filtered back-projection algorithm, which contains

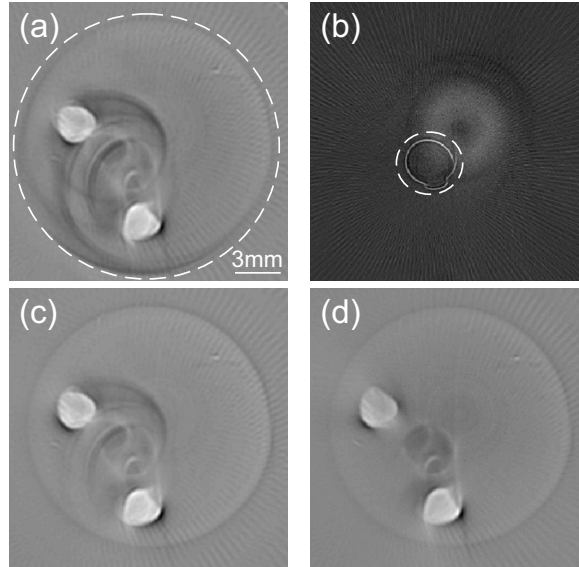


Figure 3. Tomographic reconstructions of the phantom used in the experiment. (a) Optoacoustic reconstruction obtained with the classical filtered back-projection algorithm (Eq. 4). (b) Reconstruction of the distribution of acoustic scatterers obtained with Eq. 13. (c) and (d) Optoacoustic reconstructions obtained with the weighted filtered back-projection algorithm (Eq. 5). In (c) $P_{r,dist}^i(t_{ij})$ is calculated with Eq. 10 by considering $\omega = 1$ and an area A enclosed in the dashed circumference shown in (a). In (d) $P_{r,dist}^i(t_{ij})$ is calculated with Eq. 12 by considering $\omega = 3$, an area A enclosed in the dashed circumference shown in (a) and an area B enclosed in the dashed circumference shown in (b).

strong artefacts due to reflections of the acoustic waves at the surface of the straw. A circumference enclosing the phantom can however be determined from this image (dashed white circumference in Fig. 3a). The reconstructed image of the distribution of acoustic scatterers is displayed in Fig. 3b. It was obtained with Eq. 13. From this image, the position of the points in which the acoustic wave is scattered (in this case, the surface of the straw) can be estimated. Thus, we can estimate an area covering all the acoustic scatterers (area limited by the dashed white circumference in Fig. 3b). Figs. 3c and 3d display the tomographic reconstructions obtained with the weighted filtered back-projection algorithm described in section 2.2. In Fig. 3c, the reconstruction was made by assuming that the optical absorbers and the acoustic scatterers are randomly located inside the dashed circumference of Fig. 3a, so that $P_{r,dist}^i(t_{ij})$ was estimated with Eq. 10 by considering $\omega = 1$. In Fig. 3d, we assumed that the location of the acoustic scatterers can be more accurately determined, specifically we considered that they are randomly located inside the dashed circumference of Fig. 3b. In this way, $P_{r,dist}^i(t_{ij})$ was estimated with Eq. 12 by considering $\omega = 3$. As shown in Ref. 10, the artefacts due to reflections of the acoustic waves are further reduced if some information of the distribution of scatterers is available, specifically those artefacts located close to the middle of the image. With the method introduced in this work, the information retrieved on the distribution of acoustic scatterers could be used to improve the tomographic reconstructions obtained with the statistically weighted filtered back-projection algorithm.

5. CONCLUSIONS

In this work, we have introduced a procedure to measure the distribution of acoustic scatterers in a sample being measured with a tomographic optoacoustic setup. It is based on the measurement of the waves generated at a strong optical absorber and scattered within the sample. For this, a black hair is introduced in between the sample and the transducer used to collect the optoacoustic signals. The hair is positioned in a way that the acoustic waves generated at this absorber and scattered within the sample arrive at the position of the transducer after the waves generated within the sample that propagate directly until the measuring point. Then, the part of the signal corresponding to the waves generated at the point absorber and scattered within the sample can be isolated from the rest of the signal, and the same signal can be used to estimate the distribution of acoustic scatterers and to perform the optoacoustic reconstruction itself. Furthermore, the information obtained about

the acoustic scatterers location can be used to modify the optoacoustic reconstruction algorithm in order to avoid artefacts in the images caused by the internal scattering and reflection of the acoustic waves. For this, we used a modification of the filtered back-projection algorithm in which the contribution of a signal measured at a given point at a given instant is weighted with the probability that it is not distorted due to reflected or scattered waves. Such probability can be more accurately estimated if some *a priori* knowledge on the distribution of acoustic scatterers is available. The experimental results obtained with a tissue-mimicking phantom in which a straw filled with air was included in order to cause scattering of the acoustic waves indicate a good performance of the procedure. Thus, the distribution of scatterers (the surface of the straw in this case) can be reconstructed, and the optoacoustic reconstructions of the phantoms obtained by using this information have less artefacts than the optoacoustic reconstructions obtained when this information is not available.

ACKNOWLEDGMENTS

D.R. acknowledges support from the German Research Foundation (DFG) Research Grant (RA 1848/1) and the European Research Council (ERC) Starting Grant. V.N. acknowledges support from the ERC Advanced Investigator Award and the German Ministry of Education (BMBF) Innovation in Medicine Award.

REFERENCES

- [1] Ntziachristos, V., "Going deeper than microscopy: the optical imaging frontier in biology," *Nature Methods* **7**(8), 603–614 (2010).
- [2] Wang, X., Pang, Y., Ku, G., Xie, X., Stoica, G., and Wang, L. V., "Noninvasive laser-induced photoacoustic tomography for structural and functional *in vivo* imaging of the brain," *Nature Biotechnology* **21**(7), 803–806 (2003).
- [3] Razansky, D., Distel, M., Vinegoni, C., Ma, R., Perrimon, N., Köster, R. W., and Ntziachristos, V., "Multispectral opto-acoustic tomography of deep-seated fluorescent proteins *in vivo*," *Nature Photonics* **3**(7), 412–417 (2009).
- [4] Kruger, R. A., Liu, P., Fang, Y., and Appledorn, C. R., "Photoacoustic ultrasound PAUS - reconstruction tomography," *Medical Physics* **22**(10), 1605–1609 (1995).
- [5] Köstli, K. P., Frauchiger, D., Niederhauser, J. J., Paltauf, G., Weber, H. P., and Frenz, M., "Optoacoustic imaging using a three-dimensional reconstruction algorithm," *IEEE Journal of Selected Topics in Quantum Electronics* **7**(6), 918–923 (2001).
- [6] Norton, S. J. and Vo-Dinh, T., "Optoacoustic diffraction tomography: analysis of algorithms," *Journal of the Optical Society of America A* **20**(10), 1859–1866 (2003).
- [7] Xu, M. and Wang, L. V., "Universal back-projection algorithm for photacoustic computed tomography," *Physical Review E* **71**(1), 016706 (2005).
- [8] Xu, Y. and Wang, L. V., "Effects of acoustic heterogeneity in breast thermoacoustic tomography," *IEEE Transactions on Ultrasonics, Ferroelectrics and Frequency Control* **50**(9), 1134–1146 (2003).
- [9] Deán-Ben, X. L., Ma, R., Razansky, D., and Ntziachristos, V., "Statistical approach for optoacoustic image reconstruction in the presence of strong acoustic heterogeneities," *IEEE Transactions on Medical Imaging* **30**(2), 401–408 (2011).
- [10] Deán-Ben, X. L., Ntziachristos, V., and Razansky, D., "Statistical optoacoustic image reconstruction using a-priori knowledge on the location of acoustic distortions," *Applied Physics Letters* (2011). DOI:10.1063/1.3564905.
- [11] Gusev, V. E. and Karabutov, A. A., [*Laser Optoacoustics*], American Institute of Physics, New York (USA) (1993).
- [12] Wang, X., Xu, Y., Xu, M., Yokoo, S., Fry, E. S., and Wang, L. V., "Photoacoustic tomography of biological tissues with high cross-section resolution: Reconstruction and experiment," *Medical Physics* **29**(12), 2799–2805 (2002).
- [13] Ma, R., Taruttis, A., Ntziachristos, V., and Razansky, D., "Multispectral optoacoustic tomography (MSOT) scanner for whole-body small animal imaging," *Optics Express* **17**(24), 21414–21426 (2009).